文章编号： 1007-8827(2017)04-0311-08

锂电负极用 SiO_2@碳-石墨烯杂化材料的制备

尹令红， 吴明铂， 李彦鹏， 吴桂良， 王元坤， 王 阳
(中国石油大学 重质油国家重点实验室,山东 青岛 266580)

摘 要： 采用超声辅助的水热法及后续热处理法,将硅溶胶、蔗糖、氧化石墨烯自组装制备出具有优异电化学性能的 SiO_2@碳-石墨烯(SiO_2@C-G)杂化物。结果表明:SiO_2 与蔗糖的质量比是影响 SiO_2@C-G 杂化物电化学性能的重要因素。15-SiO_2@C-G 杂化物(SiO_2 与蔗糖的质量比为 0.15),表现出较好的可逆储锂性能。电流密度为 100 mA·g^{-1},首次放电比容量为 906 mAh·g^{-1},循环 216 次后,该电极材料的放电比容量可保持在 542 mAh·g^{-1}。优异的循环稳定性及可逆容量归因于杂化物良好的导电性,SiO_2 颗粒较小的尺寸及均匀分布三者之间的协同效应。该文提出的方法有望为导电性差的金属氧化物基电极材料提供一种简单环保的制备策略。

关键词： 硅溶胶；蔗糖；石墨烯；负极；锂离子电池
中图分类号： TQ127.1$^+$1 **文献标识码：** A

基金项目:国家自然科学基金(U1662113, 51572296, 51372277)；中央高校基本科研业务费专项资金(15CX08005A).
通讯作者:吴明铂,教授. E-mail: wumb@upc.edu.cn
作者简介:尹令红,硕士研究生. E-mail: linghong1990@163.com

Synthesis of SiO_2@carbon-graphene hybrids as anode materials of lithium-ion batteries

YIN Ling-hong, WU Ming-bo, LI Yan-peng, WU Gui-liang, WANG Yuan-kun, WANG Yang
(*State Key Laboratory of Heavy Oil Processing*, *College of Chemical Engineering*, *University of Petroleum*, *Qingdao* 266580, *China*)

Abstract: SiO_2@carbon-graphene (SiO_2@C-G) hybrids with excellent electrochemical performance were prepared by the self-assembly of colloidal silica, sucrose and graphene oxide followed by ultrasonic-assisted hydrothermal and heat treatments. The mass ratio of silica to sucrose is crucial to the electrochemical performance of the resulting hybrids. A hybrid with a mass ratio of silica to sucrose of 0.15 shows the best reversible lithium storage performance, delivering an initial discharge capacity of 906 mAh·g^{-1} and a capacity of 542 mAh·g^{-1} at the 216th cycle at a current density of 100 mA·g^{-1}. The excellent cycling ability and high reversible capacity are attributed to a synergetic effect of the good conductivity of the SiO_2@C-G hybrids, the small SiO_2 particle size and the good dispersion of SiO_2 nanoparticles in the hybrids. This methodology may provide a simple, scalable and eco-friendly strategy to prepare superior electrode materials from cheap and low electrical conductivity metal oxides.
Keywords: Colloidal silica; Sucrose; Graphene; Anode; Li-ion batteries

Received date: 2017-03-15; *Revised date*: 2017-08-10
Foundation item: National Natural Science Foundation of China (U1662113, 51572296, 51372277); Fundamental Research Fund for the Central Universities (15CX08005A).
Corresponding author: WU Ming-bo, Professor. E-mail: wumb@upc.edu.cn
Author introduction: YIN Ling-hong, Master Student. E-mail: linghong1990@163.com.
English edition available online ScienceDirect (http://www.sciencedirect.com/science/journal/18725805).
Supplementary data associated with this article can be found in the online version.
DOI: 10.1016/S1872-5805(17)60124-0

1 Introduction

Lithium-ion secondary batteries (LIBs) have become the predominant power source for portable electronics in the past several decades owing to their high energy density, long lifespan and environmental benignity[1-3]. As we all know, anode material as a critical component of LIBs plays an essential role in determining electrochemical performance. Unfortunately, the commonly used graphite anode has a theoretical capacity of only 372 mAh·g^{-1}, which is far from satisfying the requirement of LIBs with high capacities. Therefore, elaborate efforts have been made to explore alternative electrode materials (e.g. Sb, Sn, Si or Ge) to meet the increasing demands for high en-

ergy density[4].

Among these feasible substitutes, the electrochemical reactivity of silica (SiO_2) has been drawn more attention owing to its low cost, high safety and high theoretical capacity. However, the large-scale practical applications of SiO_2 are restricted due to its strong Si-O bond and poor electrical conductivity during Li^+ insertion-extraction process. These main obstacles render SiO_2 electrode a low reactivity in alloying with lithium. In addition, the volume variation of SiO_2 is still harmful to its structural stability despite the lower volume expansion/shrinkage than pure silicon during cyclic process[5]. To overcome above shortcomings, nanostructured SiO_2 and SiO_2 composites in amorphous states have been constructed with the purpose of improving the reactivity with Li during cycling[6-8]. An overall improvement in the electrochemical performances of SiO_2/carbon composites can be achieved owing to the added carbon matrix, which enables an excellent buffering effect of volume change and enhances the electrical conductivity of SiO_2 electrode[9-13].

Due to natural abundance, low price and reproducibility, sucrose is widely used as a carbon precursor that is pyrolyzed under high temperatures (e. g. 900 to 1 600 ℃) to make carbon matrix[11-14]. However, the pyrolysis under high temperatures not only increases the manufacturing cost but also hinders the dispersion of SiO_2 nanoparticles (NPs), which is unfavorable for the improvement of electrical conductivity. Therefore, it still remains a challenge to find an effective way to achieve both the uniform dispersion of SiO_2 NPs and the conductive sucrose-based carbon matrix at a relatively low pyrolysis temperature.

Graphene is an attractive two-dimensional carbon material owing to its intrinsic properties such as superior electronic conductivity, high theoretical surface area (over 2 600 $m^2 \cdot g^{-1}$), high surface-to-volume ratio and amazing chemical stability. Based on these excellent properties, graphene plays an important role in constructing composites. To the best of our knowledge, SiO_2@ carbon-graphene composites have rarely been reported. Considering the cost of actual application, the content of graphene in electrode materials should be controlled at a reasonable range. Our research group has reported that 1.5% graphene in the carbon-coated tin dioxide could effectively improve the cycling performance of SnO_2-based anode materials in LIBs[15]. Therefore, it is quite important to seek a facile and scalable strategy to synthesize applicable composites that can reliably improve the cyclic performance of SiO_2/carbon nanostructures with the presence of graphene.

Herein, a facile and scalable strategy was proposed to fabricate homogeneous sucrose-based carbon-coated SiO_2 NPs composited with graphene. SiO_2@ carbon-graphene (SiO_2@ C-G) hybrids were economically obtained via the self-assembly of sucrose, graphene oxide (GO), and colloidal silica without using any organic solvent. When used as the anode materials in LIBs, the SiO_2@ C-G hybrids exhibit a significantly improved cycling performance. Simultaneously, the effect of mass ratio of SiO_2 to sucrose on the electrochemical performance was systematically investigated.

2 Experimental

2.1 Materials

All chemicals were of analytical grade and used without further purification. Graphite oxide was synthesized by the modified Hummers method[16]. SiO_2 @ C-G hybrid was prepared via hydrothermal method. Different quantities (0, 1.875, 3.750, 5.625 g) of colloidal silica (40% in water, Sigma Aldrich) and 5 g sucrose were dissolved in deionized water to obtain solutions with different mass ratios of silica/sucrose. 75 mg graphite oxide was then added into above solutions and ultrasonically treated for 3 h (700 W). The obtained suspensions were transferred to a 100 mL Teflon-sealed autoclave and kept at 190 ℃ for 12 h. After the autoclave was cooled to room temperature naturally, black products were collected by washing with distilled water and ethanol for several times, followed by drying at 60 ℃. Finally, SiO_2@ C-G hybrids were obtained after calcination at 700 ℃ for 2 h in N_2 flow with a heating rate of 5 ℃·min^{-1}. Pure SiO_2 was obtained from 15-SiO_2@ C-G by calcination at 700 ℃ in air for 2 h with a ramp heating rate of 5 ℃·min^{-1} to burn off carbon.

The mass ratios of silica to sucrose in different samples are 0, 0.15, 0.30, 0.45, which were labelled as 0-SiO_2@ C-G, 15-SiO_2@ C-G, 30-SiO_2@ C-G, 45-SiO_2@ C-G, respectively.

2.2 Characterizations

The microstructures and morphologies of the samples were characterized by X-ray diffraction (XRD, X'Pert PRO MPD, Holland), field emission scanning electron microscopy (FE-SEM, Hitachi S-4800, Japan) equipped with an energy dispersive X-ray spectrometer (EDS, EMAX 7593-H, Horiba, Japan) and transmission electron microscopy (TEM, JEM-2100UHR, Japan). The weight loss versus temperature was obtained by thermogravimetric analysis (TGA, Netzsch STA 449C, Germany) in air. Ra-

man spectroscopy was performed with a Renishaw in-Via 2000 Raman microscope. The functional groups in the samples were characterized by Fourier transform infrared spectrometry (FT-IR, Thermo Nicolet NEXUS 670, USA). Brunauer-Emmet-Teller (BET) specific surface area was calculat calculated from nitrogen adsorption/desorption isotherms using automatic specific surface area measuring equipment (ASAP 2020, America).

2.3 Electrochemical measurements

The electrochemical performances of the synthesized SiO_2@ C-G hybrids were evaluated using two-electrode half-cells. Working electrodes were prepared by mixing 60% active material, 20% carbon black and 20% binder containing poly (acrylic acid) (PAA) and sodium carboxymethyl cellulose (CMC) (1∶1) dissolved in N-methyl-2-pyrrolidinone. The above slurry was coated on Cu foil, then dried at 150 ℃ under vacuum for 2 h to remove the solvent before pressing. Finally, the electrodes were cut into disks, and a CR2032 cell was assembled in an argon-filled glove box, using lithium metal as both the counter and reference electrode, microporous polypropylene as the separator, and 1 M $LiPF_6$ solution in a mixture of ethylene carbonate and dimethyl carbonate (EC/DMC, 1∶1 v/v) as electrolyte. Galvanostatic charge-discharge cycles were tested by a LAND CT2001A cycler at current densities of 100 ~ 300 mA $\cdot g^{-1}$ within a cut-off voltage window of 0.005-2.5 V vs. Li/Li^+ at room temperature. Cyclic voltammetry (CV) curves at a scan rate of 0.2 mV $\cdot s^{-1}$ and electrochemical impedance spectra (EIS) (signal amplitude, 10 mV; frequency range, 0.01-100 000 Hz) were measured on an Ametek PARSTAT4000 electrochemistry workstation.

3 Results and discussion

Fig. 1(a) shows a typical SEM image of the 15-SiO_2@ C-G hybrid, the structure of continuous graphene can be seen from the right side. The content of carbon, oxygen and silicon in the 15-SiO_2@ C-G hybrid was further investigated by EDS elemental mapping analyses, which are displayed as red, green and blue in the insertion, respectively. The uniform distributions of these three elements on the selected regions suggest the good dispersibility of silica in the 15-SiO_2@ C-G hybrid. From the TEM image (Fig. 1(b)), the curly and wrinkled morphology of graphene and carbon layer in the 15-SiO_2@ C-G hybrid can be easily observed. Meanwhile, only a few SiO_2 NPs are found embedded in the superficial surface of graphene and carbon layer. The diameter of silica NPs is about 14 nm and the selected-area electron diffraction (SAED) pattern (see Fig. S1) reveals that silica in the composite is amorphous. 0-SiO_2 @ C-G without SiO_2 exhibits the similar layer structure as shown in Fig. 1(c). The SiO_2/carbon composites synthesized by hydrothermal method without adding GO are usually spherical structure[17]. Obviously, GO exerts essential effect on the construction of the continuous layer structure. To further illuminate the structure, the 15-SiO_2@ C-G was calcined at 700 ℃ in air to obtain the pure SiO_2. Fig. 1(d) shows the SEM image of the pure SiO_2 phase, which partly collapses and agglomerates in absence of carbon skeleton support. This collapse is likely caused by the cancelling stress exerted from the graphene and carbon layer via calcination in air at 700 ℃. TGA result in Fig. S2 suggests that the major weight loss in air happen in the temperature range of 400-640 ℃, which means only pure SiO_2 is left after the calcination of the 15-SiO_2@ C-G hybrid in air at 700 ℃. These phenomena suggest that the structure of SiO_2@ C-G hybrid should be quite elastic, which might be advantages for improving cycling performance.

The crystal textures and structural information of the 15-SiO_2@ C-G and pure SiO_2 are revealed by X-ray diffraction (XRD). As shown in Fig. 2(a), pure SiO_2 phase with a broad peak indicates the amorphous structure of SiO_2, which is in line with SAED pattern shown in Fig. S1(b). The peak of SiO_2 in the 15-SiO_2 @ C-G hybrid is overlapped by a wide peak around 23°, which is assigned to the (002) diffraction plane of hexagonal graphite. A weak peak also appears around 43°, which is the characteristic of (100) h-graphite plane. No peak indexed to silicon can be found in the 15-SiO_2 @ C-G hybrid, demonstrating that no SiO_2 is reduced to Si by carbonization in N_2 at 700 ℃, which is accordant with literature[11]. The interlayer spacing of (002) graphite plane in the 15-SiO_2@ C-G is about 0.386 nm, which is attributed to the disordered graphite with stacked layer structures[18]. Raman spectra of 0-SiO_2@ C-G, the 15-SiO_2@ C-G, 30-SiO_2@ C-G and 45-SiO_2@ C-G hybrids are displayed in Fig. 2(b). The two obvious characteristic peaks around 1 320 and 1 580 cm^{-1} are ascribed to the typical Raman mode of *D* band and *G* band of carbon, respectively. *D* band can be ascribed to structural defects and disordered carbon, while *G* band corresponds to the structural integrity of graphite[19, 20]. The I_D/I_G ratio of the 15-SiO_2@ C-G hybrid is 1.064, higher than 1.061 of 0-SiO_2@ C-G, 0.907 of 30-SiO_2@ C-G and 0.950 of 45-SiO_2@ C-G. Compared with 0-SiO_2 @ C-G, blue shifts of *D*

and *G* bands in the 15-SiO_2@C-G, 30-SiO_2@C-G and 45-SiO_2@C-G can be seen, which are consistent with the introduction of different amounts of SiO_2 NPs. In addition, the contents of graphene in samples are also different and can be estimated approximately by the following equation:

$$\text{Graphene}\% = \frac{m_{GO}}{m_{SiO_2}+m_{GO}+m_{sucrose}}$$

According to the formula, the content of graphene in 0-SiO_2@C-G, the 15-SiO_2@C-G, 30-SiO_2@C-G and 45-SiO_2@C-G are about 1.48%, 1.29%, 1.14% and 1.02%, respectively. 15-SiO_2@C-G hybrid with the highest I_D/I_G ratio indicates that a proper content of graphene leads to abundant defects, which can not only enhance the fast diffusion of Li^+ but also provide more reversible sites for Li^+ storage, and thus improve the electrochemical performance.

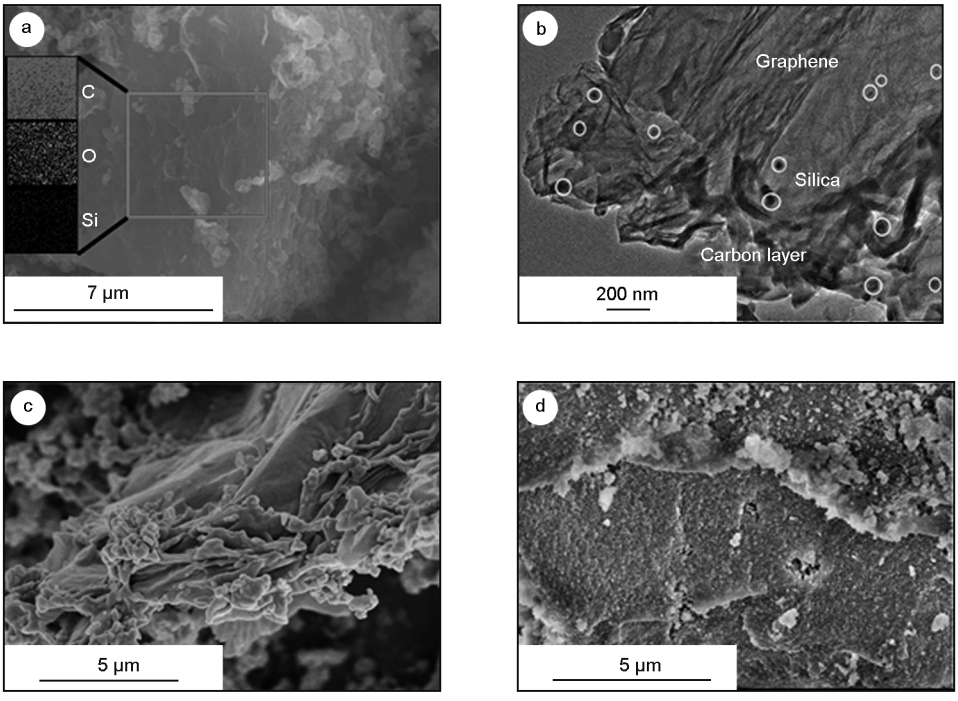

Fig. 1 SEM images of (a) 15-SiO_2@C-G and corresponding elemental mapping images of carbon, oxygen, and silicon in the selected area (pink rectangle), (c) 0-SiO_2@C-G and (d) pure SiO_2 obtained by calcination at 700 ℃ in air, and (b) TEM image of 15-SiO_2@C-G.

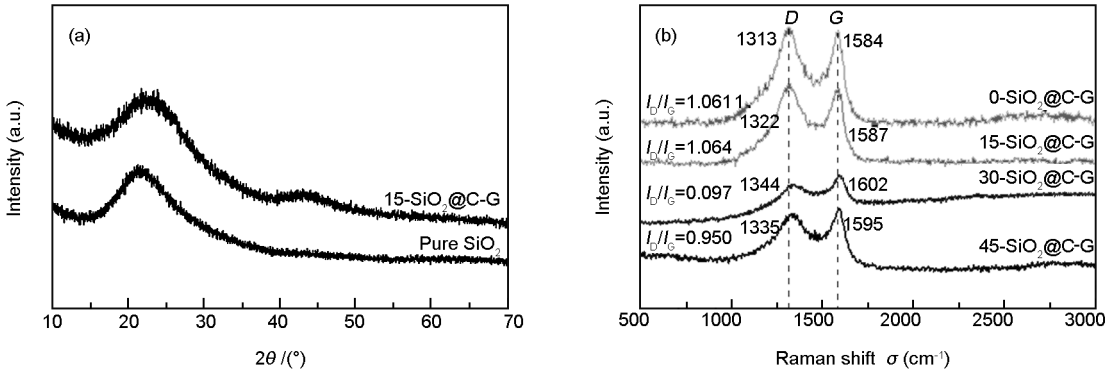

Fig. 2 (a) XRD patterns of the 15-SiO_2@C-G and pure SiO_2 and (b) Raman spectra of 0-SiO_2@C-G, 15-SiO_2@C-G, 30-SiO_2@C-G and 45-SiO_2@C-G hybrids.

In order to further understand the decoration of SiO_2 in SiO_2@C-G hybrids and to evaluate the reduction of GO in SiO_2@C-G hybrids, FT-IR spectra of 0-SiO_2@C-G, the 15-SiO_2@C-G, 30-SiO_2@C-G and 45-SiO_2@C-G hybrids are given in Fig. 3(a). With increasing content of silica, the peak at 1 102 cm^{-1} attributing to asymmetry Si—O—Si bond stretching vibration becomes narrow and strong,

which may be caused by the superfluous SiO_2 NPs. In addition, it is well known that the electrical conductivity of GO is poor due to the presence of a large amount of oxygen functional groups (Fig. S3). Once such species are removed, the high electronic conductivity of graphene sheets is deemed to be resumed[21-23]. Most oxygen-related groups including —OH (3 441 cm^{-1}), C═O in COOH (1 735 cm^{-1}) and C—O (1 055 cm^{-1}) stretching vibrations assigned to GO are almost eliminated after calcination at 700 ℃ in N_2[24]. All above results verify that most GO has been reduced to graphene and SiO_2 has been decorated successfully in SiO_2@C-G hybrids.

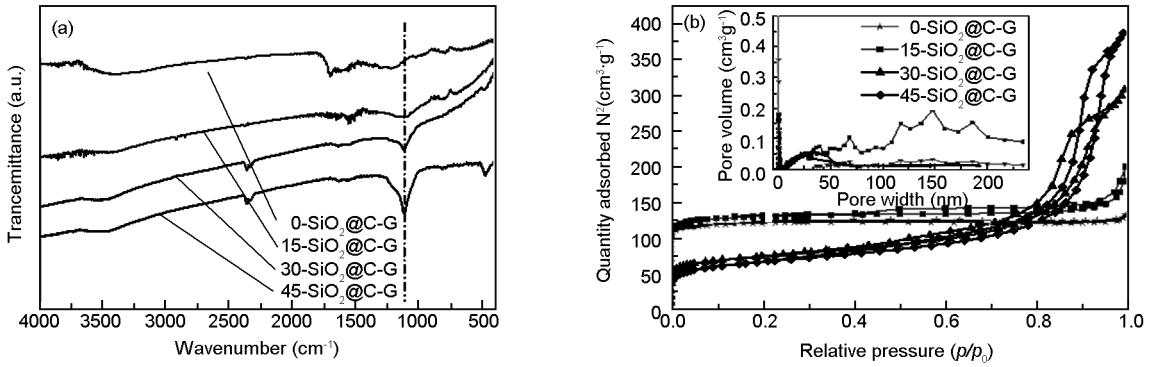

Fig. 3 (a) FT-IR spectra and (b) nitrogen adsorption-desorption isotherms and pore-size distributions of 0-SiO_2@C-G, 15-SiO_2@C-G, 30-SiO_2@C-G and 45-SiO_2@C-G hybrids.

The N_2 adsorption-desorption isotherms together with pore size distributions of 0-SiO_2@C-G, the 15-SiO_2@C-G, 30-SiO_2@C-G and 45-SiO_2@C-G hybrids are given in Fig. 3(b). All samples show a typical type-IV curve and have hysteresis loops which reveal the presence of mesopores. It is interesting to note that the hysteresis loops of SiO_2@C-G hybrids are obviously different at different mass ratios of silica/sucrose. The pore size distribution inserted in Fig. 3(b) further indicates that 0-SiO_2@C-G is microporous and the introduction of silica leads to the formation of mesopores. It can be noticed that the 15-SiO_2@C-G also possesses abundant macropores compared with the other SiO_2@C-G hybrids. The macropores may come from the layer space of the 15-SiO_2@C-G hybrid. Although no activation is employed, the BET surface area of the 15-SiO_2@C-G hybrid is as high as 483.6 $m^2 \cdot g^{-1}$. The formation of the porous structure in the 15-SiO_2@C-G hybrid is primarily caused by thermal decomposition of oxygen-containing groups, accompanied by releasing a large amount of CO_2, CO and H_2O. The diffusion of these gases can develop channels in the 15-SiO_2@C-G hybrid, forming numerous pores. Meanwhile, the large surface energy of single-layer graphene is accumulated, making graphene folded to develop into a slit type pore structure. The structure with a large specific surface area and abundant pores can benefit the accessibility of electrolyte, the fast diffusion of lithium ions, and the structure stability of the composites. Meanwhile, it can provide more active space for accommodating lithium ions (such as the edge of space and nanopores)[25].

To evaluate the electrochemical activity of SiO_2-based hybrids in Li^+ storage, the samples are used as anodes for LIBs. Fig. 4 shows the galvanostatic discharge (Li insertion)/charge (Li extraction) voltage profiles of the 15-SiO_2@C-G at a current density of 100 $mA \cdot g^{-1}$ in the voltage window of 0.005-2.5 V for different cycles. The 15-SiO_2@C-G electrode delivers a high specific discharge capacity of 906 $mAh \cdot g^{-1}$ for the first cycle.

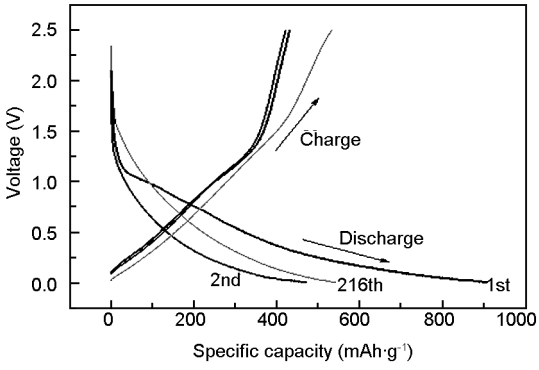

Fig. 4 Charge/discharge potential profiles of the 15-SiO_2@C-G at the 1st, 2nd, 216th cycles.

The coulombic efficiency of the 15-SiO_2@C-G hybrid is shown in Fig. S4, the initial coulombic efficiency (47.6%) indicates that the large irreversible capacity loss should be attributed to the formation of SEI film[26] and generation of Li_2O and Li_4SiO_4 in irreversible electrochemical reactions. In the subsequent

cycles, the coulombic efficiency of the second cycle rises to 89.5% and continues to increase in the following cycles to about 99%. The mechanism of electrochemical reaction between SiO_2 and Li might depend on the microstructure[5-8, 27]. Here, to better illustrate the mechanism of the electrochemical reaction happened in SiO_2@C-G hybrids, the cyclic voltammogram (CV) of SiO_2@C-G electrodes were performed at a scan rate of 0.2 $mV \cdot s^{-1}$ in the voltage range of 0.005-2.5 V as shown in Fig. 5. The CV profiles of different SiO_2@C-G hybrids are similar. In the first cycle, the large broad reduction peaks around 0.3-1.6 V (Fig. 5(a)) change into small peaks and become sharp with increasing silica amount as shown in Fig. 5(b-d), which indicates that the amorphous SiO_2 in SiO_2@C-G hybrids is active and can participate in electrochemical reactions. The obvious irreversible reduction peaks above 0.75 V are attributable to the electrolyte decomposition and the formation of solid electrolyte interface (SEI) layer on the surface of electrodes. The cathodic peak below 0.5 V is related to the lithiation of SiO_2@C-G hybrids, as described in Eq. (a-c). With increasing mass ratio of silica/sucrose, the anodic peak centered at 0.2 V become narrow, indicating the Li-extraction process of as-formed Li–Si alloy. The carbon component and in-situ formed Si are electrochemically reactive, which contribute a certain amount of reversible capacity (Eq. (b-c)) during the reversible alloying/de-alloying with lithium. From the second cycle, CV curves become nearly stable and show mainly the reversible behavior of amorphous silicon and disordered carbon (Eq. (b-c)), which implies the good cycling performance of SiO_2@C-G hydrids.

$$2SiO_2+4Li^++4e^-\rightarrow Li_4SiO_4+Si;$$
$$SiO_2+4Li^++4e^-\rightarrow 2Li_2O+Si \quad (a)$$
$$Si+xLi^++xe^-\leftrightarrow Li_xSi \quad (b)$$
$$6C+yLi^++ye^-\leftrightarrow Li_yC_6 \quad (c)$$

The cycling performances of 0-SiO_2@C-G, the 15-SiO_2@C-G, pure SiO_2 electrodes at the current density of 100 $mA \cdot g^{-1}$ are shown in Fig. 6(a). Compared with 0-SiO_2@C-G and pure SiO_2 electrodes, the 15-SiO_2@C-G electrode presents the highest reversible capacity and the most excellent cycling stability. The discharge specific capacity slightly decreases from the 2nd cycle till the 16th cycle, and then gradually increases to 542 $mAh \cdot g^{-1}$ at the 216th cycle. The 0-SiO_2@C-G decreases gradually and remains only 220 $mAh \cdot g^{-1}$ at the 216th cycle. Cycling performances of 30-SiO_2@C-G and 45-SiO_2@C-G are also compared and given in Fig. S5. 30-SiO_2@C-G, 45-SiO_2@C-G and pure SiO_2 electrodes display similar growth trend but increase extremely slow compared with the 15-SiO_2@C-G electrode. The electrochemical performances of SiO_2@C-G hybrids with different amounts of SiO_2 are different and can be explained as follows. With increasing amount of SiO_2, the aggregation of abundant SiO_2 NPs deteriorates the electrochemical performance. The suitable content of graphene could lead to an excellent electrochemical performance. The obviously higher capacity of the 15-SiO_2@C-G than the others may be caused by the deformation of a polymer gel-like conductive film[28-30] or activated process to make full use of the well coated silica NPs, which increase the amount of silicon generated during the electrochemical reaction. Moreover, it could be ascribed to the unique porous structure. The continuous carbon frame is beneficial to provide more active sites for Li^+ storage and advantageous to Li^+ diffusion and transport. In addition, SiO_2 NPs can be homogeneously dispersed by amorphous carbides and the formed C-G web can buffer the volume variation to some extent.

More analyses have been carried on the 15-SiO_2@C-G electrode with the best electrochemical performance. As shown in Fig. 6(b), the 15-SiO_2@C-G electrode exhibits a good rate performance at the current densities of 100, 200 and 300 $mA \cdot g^{-1}$. When the current density is increased to 200, 300 $mA \cdot g^{-1}$, it delivers a discharge capacity of 449 and 341 $mAh \cdot g^{-1}$, respectively. Moreover, the capacity rebounds back to 405 $mAh \cdot g^{-1}$ at 100 $mA \cdot g^{-1}$, which is still higher than 372 $mAh \cdot g^{-1}$ of graphite theoretical capacity, indicating the better rate performance and the enhanced cycling stability of the 15-SiO_2@C-G.

In order to better reveal the enhanced electrical conductivity of the 15-SiO_2@C-G electrode with increasing cycle number, electrochemical impedance spectroscopic (EIS) measurements were carried out. Fig. 7 shows the Nyquist plots of the 15-SiO_2@C-G electrode before and after 5 and 300 cycles. The EIS spectra show a semicircle at the high-to-medium frequency region, corresponding to the charge transfer resistance. A straight line at the low frequency region represents the diffusion resistance. It is noted that the charge transfer resistance of the 15-SiO_2@C-G electrode even becomes small with increasing cycles, which is probably due to the formation of Si nanoparticles during electrochemical reactions. In addition, the continuous and conductive graphene network in the 15-SiO_2@C-G (~1.29%) further strengthens the structural integrity, which could facilitate the fast charge transport between the electrode and the electrolyte, thus leading to an excellent cyclic stability and rate performance.

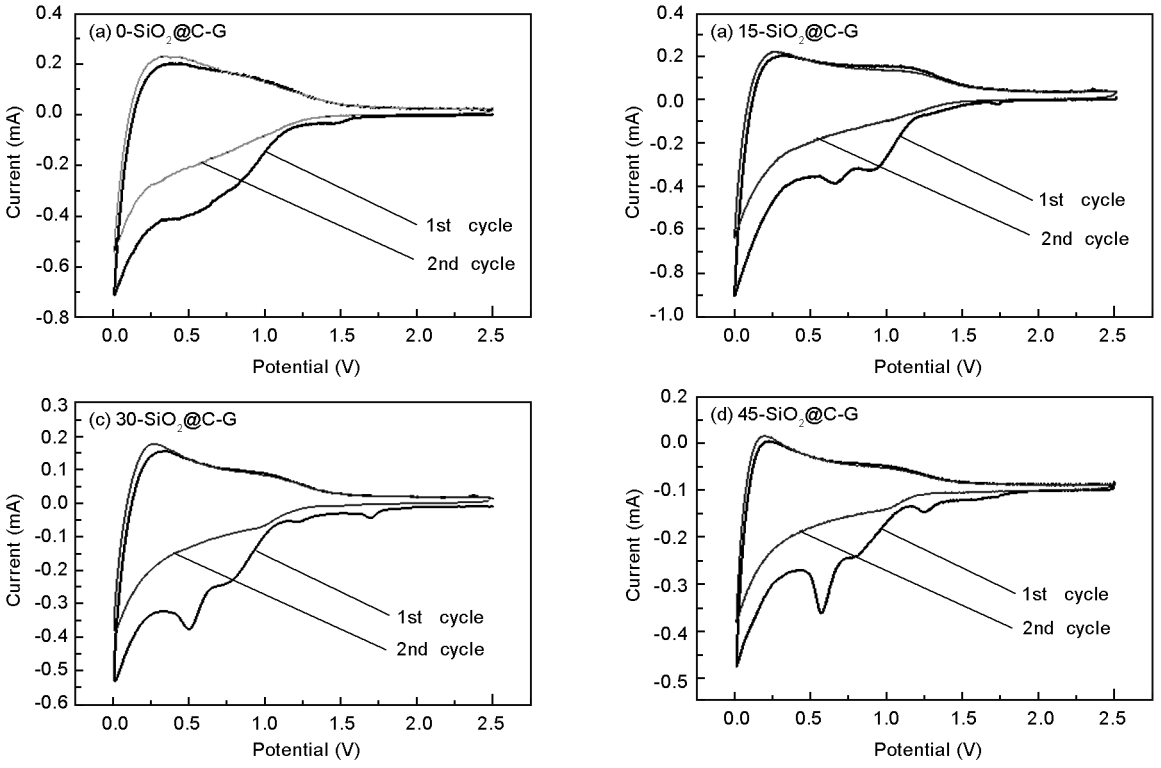

Fig. 5　Cyclic voltammograms of a half-cell composed of electrode materials vs. Li/Li^+ at a scan rate of 0.2 $mV \cdot s^{-1}$ during the first 2 cycles: (a) 0-SiO_2@C-G, (b) 15-SiO_2@C-G, (c) 30-SiO_2@C-G and (d) 45-SiO_2@C-G.

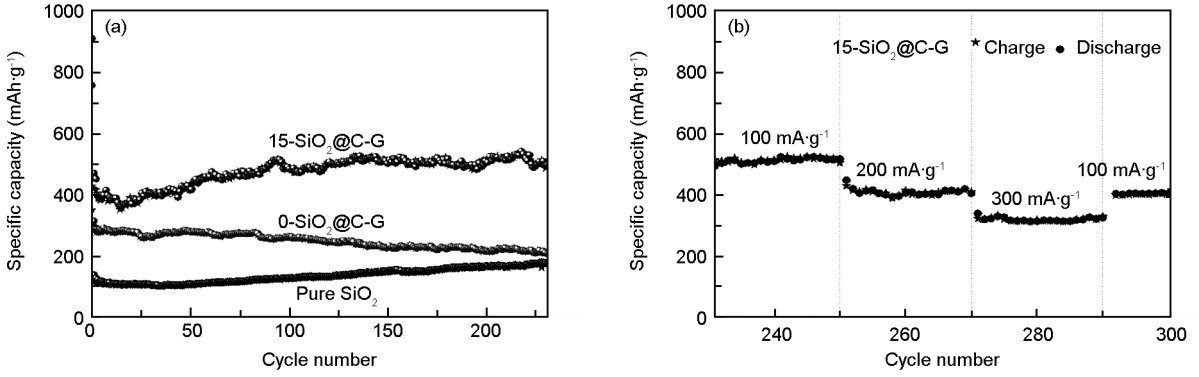

Fig. 6　(a) Discharge-charge curves of 0-SiO_2@C-G, 15-SiO_2@C-G and pure SiO_2 cycled between 0.005 and 2.5 V at a current density of 100 $mA \cdot g^{-1}$. (b) Cycling performance of the 15-SiO_2@C-G cell at various current densities.

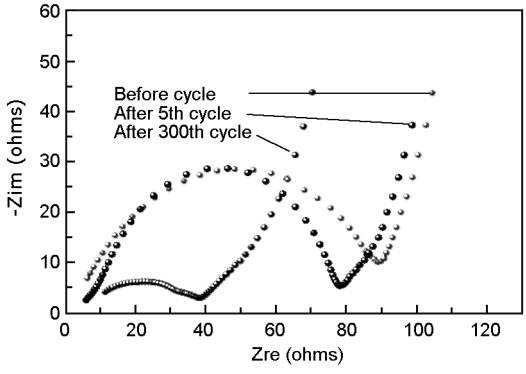

Fig. 7　Electrochemical impedance spectra of the 15-SiO_2@C-G hybrid after different cycles in the frequency range between 100 kHz and 10 mHz.

4　Conclusions

SiO_2@ carbon-graphene hybrids have been successfully prepared via the self-assembly of colloidal silica, sucrose and graphene oxide in successive ultrasonic, hydrothermal and heat treatments. The results prove that graphene plays an important role in the construction of SiO_2@C-G hybrids, which can effectively improve the cyclic performance and enhance the structural stability of carbon-coated silica composites as anode materials in LIBs. The convenient fabrication and unique structure together with conductive carbon support of SiO_2@C-G remarkably enhance the

electrical conductivity of SiO_2, thus improves the electrochemical performance. The as-made SiO_2@C-G hybrids with super electrochemical performance hold promise as electrode materials.

References

[1] Tarascon J M, Armand M. Issues and challenges facing rechargeable lithium batteries[J]. Nature, 2001, 414: 359-367.

[2] Liu S H, Wang Z Y, Yu C, et al. A flexible TiO_2(B)-based battery electrode with superior power rate and ultralong cycle life [J]. Advanced Materials, 2013, 25(25): 3462-3467.

[3] Kaskhedikar N A, Maier J. Lithium storage in carbon nanostructures[J]. Advanced Materials, 2009, 21(25-26): 2664-2680.

[4] Liu C, Li F, Ma L P, et al. Advanced materials for energy storage[J]. Advanced Materials, 2010, 22(8): 28-62.

[5] Li M Q, Yu Y, Li J, et al. Nanosilica/carbon composite spheres as anodes in Li-ion batteries with excellent cycle stability[J]. Journal of Materials Chemistry A, 2015, 3(4): 1476-1482.

[6] Chang W S, Park C M, Kim J H, et al. Quartz (SiO_2): a new energy storage anode material for li-ion batteries[J]. Energy & Environmental Science, 2012, 5(5): 6895-6899.

[7] Sun Q, Zhang B, Fu Z W. Lithium electrochemistry of SiO_2 thin film electrode for lithium-ion batteries[J]. Applied Surface Science, 2008, 254(13): 3774-3779.

[8] Kim Y K, Moon J W, Lee J G, et al. Porous carbon-coated silica macroparticles as anode materials for lithium ion batteries: Effect of boric acid[J]. Journal of Power Sources, 2014, 272: 689-695.

[9] Lv P P, Zhao H L, Gao C H, et al. Highly efficient and scalable synthesis of SiO_x/C composite with core-shell nanostructure as high-performance anode material for lithium ion batteries[J]. Electrochimica Acta, 2015, 152: 345-351.

[10] Lv P P, Zhao H L, Wang J, et al. Facile preparation and electrochemical properties of amorphous SiO_2/C composite as anode material for lithium ion batteries[J]. Journal of Power Sources, 2013, 237: 291-294.

[11] Yao Y, Zhang J J, Xue L. G, et al. Carbon-coated SiO_2 nanoparticles as anode material for lithium ion batteries[J]. Journal of Power Sources, 2011, 196(23): 10240-10243.

[12] Guo B K, Shu J, Wang Z W, et al. Electrochemical reduction of nano-SiO_2 in hard carbon as anode material for lithium ion batteries [J]. Electrochemistry Communications, 2008, 10 (12): 1876-1878.

[13] Yang X Q, Huang H, Li Z H, et al. Preparation and lithium-storage performance of carbon/silica composite with a unique porous bicontinuous nanostructure[J]. Carbon, 2014, 77: 275-280.

[14] Luo W, Bommier C, Jian Z L, et al. Low-surface-area hard carbon anode for Na-ion batteries via graphene oxide as a dehydration agent[J]. ACS Applied Materials & Interfaces, 2015, 7 (4): 2626-2631.

[15] Li Z T, Wu G L, Liu D, et al. Graphene enhanced carbon-coated tin dioxide nanoparticles for lithium-ion secondary batteries[J]. Journal of Materials Chemistry A, 2014, 2(20): 7471-7477.

[16] Hummers W S, Offeman R E. Preparation of graphitic oxide [J]. Journal of the American Chemical Society, 1958, 80 (6): 1339-1339.

[17] Ren Y R, Wei H M, Huang X B, et al. A facile synthesis of SiO_2@C@ graphene composites as anode material for lithium ion batteries[J]. International of Journal of Electrochemical Science, 2014, 9(12): 7784-7794.

[18] Pimenta M A, Dresselhaus G, Dresselhaus M S, et al. Studying disorder in graphite-based systems by Raman spectroscopy [J]. Phys. Physical Chemistry Chemical Physics, 2007, 9 (11): 1276-1291.

[19] Luo D, Zhang G X, Liu J, et al. Evaluation criteria for reduced graphene oxide[J]. Journal of Physical Chemistry C, 2011, 115(23): 11327-11335.

[20] Sun J, Teng X Y, Yang J X, et al. One pot synthesis of a highly water-dispersible hybrid glucose carbides and reduced graphene oxide material with superior electrical capacitance[J]. Journal of Materials Science, 2013, 48(23): 8277-8286.

[21] Dreyer D R, Park S, Bielawski C W, et al. The chemistry of graphene oxide [J]. Chemical Society Reviews, 2010, 39 (12010): 228-240.

[22] Kosynkin D V, Higginbotham A L, Sinitskii A, et al. Longitudinal unzipping of carbon nanotubes to form graphene nanoribbons[J]. Nature, 2009, 458(7240): 872-877.

[23] Park S, Ruoff R S. Chemical methods for the production of graphenes[J]. Nature Nanotechnology, 2009, 4(4): 217-224.

[24] Wu G L, Wu M B, Wang D, et al. A facile method for in-situ synthesis of SnO_2/graphene as a high performance anode material for lithium-ion batteries [J]. Applied Surface Science, 2014, 315: 400-406.

[25] Wu Y P, Jiang C Y, Wan C R, et al. Effects of catalytic oxidation on the electrochemical performance of common natural graphite as an anode material for lithium ion batteries[J]. Electrochemistry Communications, 2000, 2(4): 272-275.

[26] Wu G L, Li Z T, Wu W T, et al. Effects of calcination on the preparation of carbon-coated SnO_2/graphene as anode material for lithium-ion batteries[J]. Journal of Alloys and Compounds, 2014, 615: 582-587.

[27] Gao B, Sinha S, Fleming L, et al. Alloy formation in nanostructured silicon [J]. Advanced Materials, 2001, 13 (11): 816-819.

[28] Fei H L, Peng Z W, Li L, et al. Preparation of carbon-coated iron oxide nanoparticles dispersed on graphene sheets and applications as advanced anode materials for lithium-ion batteries [J]. Nano Research, 2014, 7(4): 502-510.

[29] Zhou G, Wang D W, Hou P X, et al. A nanosized Fe_2O_3 decorated single-walled carbon nanotube membrane as a high-performance flexible anode for lithium ion batteries[J]. Journal of Materials Chemistry, 2012, 22(34): 17942-17946.

[30] Do J S, Weng C H. Preparation and characterization of CoO used as anodic material of lithium battery[J]. Journal of Power Sources, 2005, 146(1-2): 482-486.